IJHSR
ijhighschoolresearch.org
RESEARCH ARTICLE

ATHENA Science Enabled by Cryocooled Space Detectors

Hanna Cho

Yongsan International School of Seoul, 285 Itaewon-ro, Yongsan-gu, Seoul, 04347, Seoul, South Korea; chohanna1230@gmail.com

ABSTRACT: This study examines how cryogenic systems power the ATHENA mission's X-ray observations. The X-ray Integral Field Unit (X-IFU) requires cooling to 50 mK for high-resolution spectroscopy. This paper reviews key cryocoolers—Stirling, Joule-Thomson, and Adiabatic Demagnetization Refrigerators—and their roles in space applications. A detailed review of the multi-stage cryochain explains how it achieves the ultra-low temperatures needed for X-IFU. Transition Edge Sensors (TES), vital for X-ray detection, operate at the core of this system. These technologies enable ATHENA to study black hole physics, cosmic feedback, and the growth of large-scale cosmic structures. By combining advanced cooling methods with precise instrumentation, this study shows how ATHENA will deepen our understanding of the hot and energetic universe.

KEYWORDS: Physics and Astronomy, Astronomy and Cosmology, ATHENA, X-ray Astronomy, X-IFU, Space Instrumentation.

Introduction

The universe is a complex and nebulous subject to explore, filled with mysterious things that challenge our understanding. To unravel these cosmic enigmas, the Advanced Telescope for High-ENergy Astrophysics (ATHENA) mission, selected by ESA in June 2014, will explore a plethora of astronomical subjects. This includes the examination of stellar formation and evolution, supernova explosions, and gamma-ray bursts.[1] Furthermore, it will study the growth of supermassive black holes and their influence on galaxy formation and evolution. It will also explore how the universe is taking shape through the study of how baryonic matter formed large-scale structures such as supermassive black holes.[2] These black holes largely influence their surroundings through a process known as Cosmic Feedback. Therefore, X-rays are crucial to observing this hot and energetic universe as they can penetrate through obscured environments, revealing various ionization states of abundant elements.[3]

To achieve its scientific objectives, ATHENA will carry the X-ray Integral Field Unit (X-IFU) instrument, which can provide spatially resolved high-resolution spectroscopy, granting the ability to observe bright X-ray sources. X-IFU aims to tackle key scientific concepts related to the Hot and Energetic Universe and enable critical observation of the universe's chemical evolution and the physical processes behind the growth of large-scale structures. Overall, X-IFU's high-resolution X-ray spectroscopy will provide insights across a wide range of astronomical objects, from planets and stars to supernovae, compact objects, and the interstellar medium.[4]

The X-IFU consists of a large array of X-ray absorbers on top of the Transition Edge Sensors (TES). Each X-ray photon creates a distinct current pulse, with its amplitude reflecting the photon's energy. These pulses are measured by the TES microcalorimeter to sense the pulses generated by X-ray photons and determine the measurement of photon energy and arrival time. The heat capacity of the TES, the thermal conductance to the cold bath, and the electrical properties of the TES circuit all impact the shape and timing of these pulses.[3] Therefore, to accurately measure this change in electrical resistance, TES needs to be cooled to below 100 mK, with the thermal bath at 50 mK.[4] This cooling is achieved through a multi-stage cryogenic chain consisting of five 15 K pulse tube coolers, two 4 K Joule-Thomson coolers, two 2 K Joule-Thomson coolers, and a final stage Adiabatic Demagnetization Refrigeration (ADR) 100 mK, with the thermal bath at 50 mK.[5]

Many criteria must be met before cryocoolers can be approved for use in space, such as cooling power at the required cold end temperature with a reduced input power, reliable and maintenance-free operation, compactness, minimum vibration and noise, and long shelf life.[6] In addition, cryocoolers for space applications are generally qualified for a ten-year lifetime.[7] Lastly, the cost is undoubtedly an important factor, especially when maintenance opportunities are difficult, therefore, it is often justified to invest more in the initial capital cost to reduce the risk of failure.[8] Understanding the advantages and limitations of each type of cryocooler is essential for selecting the most appropriate technology for space applications, which ensures optimal performance and reliability. Therefore, this paper will focus on the various types of cryocoolers and their role in the ATHENA mission.

Background and Theory

Stirling Cryocoolers:

There are many ways to classify cryocoolers, and the primary distinguishing features are based on the types of thermodynamic cycles that are being run to achieve refrigeration: recuperative or regenerative.[9] In the recuperative cycles, the working fluid moves around a loop in one direction at fixed high and low pressures, with JT (Joule-Thomson) and Brayton cycles as prime examples of these types.[10] Due to the steady flow and pressure, temperature oscillations and vibrations

DOI: 10.36838/v7i9.37

are low. In contrast, the regenerative cycle uses an oscillating flow of gas, and its pressure cools the cold end of the system; Stirling, Gifford-McMahon, and pulse tube cycles are prime examples of such types.[11] Temperatures of 3 K up to 300 K can be achieved with regenerative cryocoolers, although temperatures below 150 K are the most common.[8]

Each cryocooler has its distinct advantages and disadvantages, and these are considered for each space mission. One of the most unique properties of pulse tube cryocoolers is the lack of a moving part; they utilize Stirling or GM-type compressors, which makes them more reliable and minimizes vibration, at the cost of reducing efficiency.[12] Therefore, pulse tube cryocoolers for space applications typically operate at high frequencies for efficiency, which makes it challenging to achieve very low temperatures due to regenerator performance degradation.[13] For single-stage coolers, temperatures have been known to reach 40-70 K,[9] but multi-stage coolers can cool to much lower temperatures.[14]

Stirling coolers were the first coolers to be successfully utilized in space and proven to be reliable and highly efficient. Recent developments of two-stage devices allow lower temperature ranges from 60-80 K down to as low as 15-30 K.[11,15] However, to reach 4 K temperatures, it is more common for Stirling cycles to be integrated with other coolers. Some of the most common pairs are Stirling and JT coolers, previously mentioned, and hybrid Stirling-type pulse tube coolers.

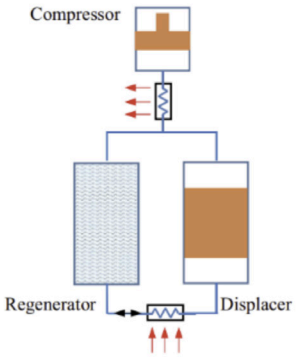

(a) Stirling/Pulse Tube

Figure 1: A schematic showing the Stirling cycle operation for a Stirling cryocooler. (Reference numbers have been modified from the original source.)[16] Figure 1 shows the four thermodynamic processes of the Stirling cycle: isothermal compression, isochoric cooling, isothermal expansion, and isochoric heating. It emphasizes how these steps enable efficient closed-cycle cryogenic cooling.

In the Stirling cycle, the flow of the working fluid, commonly helium, is controlled with the use of pistons and displacers.[16] The cycle consists of four heat transfer procedures: two isothermal and two isochoric processes. First, during isothermal compression, the fluid is compressed and the heat is transferred from the fluid to a warm heat exchanger. Next, in the constant-volume regenerative cooling phase, the heat is transferred from the fluid into the regenerative matrix through the motion of displacers, lowering the temperature. Then, during the isothermal expansion, the compressor piston and displacer move backward, expanding the gas and lowering the pressure.[17] The working fluid also absorbs heat from the required external source. Finally, in the constant volume regenerative heating phase, the gas is moved to the warm end of the cooler, and the fluid absorbs heat from the regenerative matrix, completing the cycle.[18] Figure 1 presents the schematic for the Stirling cycle as run in a Stirling cryocooler.[16]

Net cooling power is the amount of cooling power that is available for cooling the item that is attached to the cold tip.[17] This can be derived as:[19]

$$\dot{Q} = \dot{W} + \dot{H}_e - \dot{H}_i + \frac{d < U >}{dt} \quad (1)$$

Carnot efficiency is used as a standard for comparing heat engine cycles, as it represents the highest efficiency in a given temperature range.[9] For the cryocooler that operates the Stirling thermodynamic cycle, the equations can be expressed as this:[19]

$$\eta_r = (\frac{Q_c}{\dot{W}_{in}})(\frac{T_h}{T_c} - 1) \quad (2)$$

Qc represents cooling power, and the term W signifies displacer input power; the ratio is also known as the coefficient of performance, which measures how much cooling can be achieved per unit of work input. The latter part of the equation represents the temperature ratio between the hot and cold sides, as Tc is the cold end temperature while Th is the heat rejection temperature.[20]

The JT cycle:

JT cryocoolers are valued for their stability, compact structure, simplicity, reliability, and low electrical and mechanical noise levels.[15,21] Furthermore, the JT cycle, operating with no moving parts at the cold end, can easily be made compact. However, similar to the pulse tube coolers, high-efficiency heat exchangers are essential to reach cryogenic temperatures due to the temperature changes in the cycle being relatively small compared to the temperature difference between ambient and cryogenic temperatures.[13] Therefore, hybrid JT cryocoolers working at liquid helium temperature are widely used in space detectors working at 4 K due to their flexibility and relatively high efficiency.[21] Therefore, the ATHENA project is currently developing a two-stage Stirling refrigerator, which provides 4.5 K temperatures. This 20 K two-stage Stirling cryocooler, consisting of a cold head with two cold stages, is first employed as a pre-cooler, which is then connected to the JT heat exchangers so that the helium gas can be cooled below 20 K.[21]

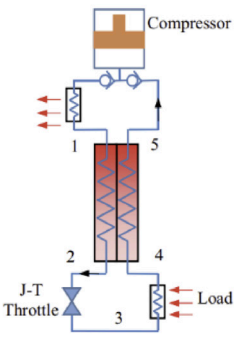

(c) Joule-Thomason

Figure 2: A schematic showing the JT cycle operation for a JT cryocooler. (Reference numbers have been modified from the original source.)[16] Figure 2 illustrates the Joule-Thomson cycle, highlighting isenthalpic expansion through a throttling valve as the core cooling mechanism. It demonstrates how high-pressure gas undergoes a temperature drop as it expands without external work.

The JT cycle achieves cooling without external heat input or work production, and therefore, expansion happens at constant enthalpy.[22] First, the high-pressure gas first passes through a primary heat exchanger, where it is precooled by transferring heat to an external cooling system.[23] The cooled, high-pressure gas undergoes isenthalpic expansion upon entering the JT orifice or a porous plug.[17] This expansion causes a pressure drop, and the temperature decreases when the gas is in the cooling region. Then, this cooled, low-pressure gas passes through a secondary heat exchanger, where it is further cooled to cryogenic temperatures.[24] Figure 2 presents the schematic for the JT cycle as run in a JT cryocooler.[16]

For recuperative cryocoolers, such as JT coolers, net cooling power is the difference between the gross cooling power produced by the expander and the losses from the heat exchanger. This is expressed as:

$$\dot{Q}_L\max = \dot{m}\left(h(T_a, p_1) - h(T_a, p_h)\right) \quad (3)$$

This equation calculates the maximum cooling power expressed through the mass flow rate (m) of the working fluid and on the enthalpy differences of the high and low-pressure fluids at constant temperature (Ta).[25]

Based on the Colburn-Chilton analogy, an analytical formula can be derived for Carnot efficiency upon considering the loss during the compression process:

$$\eta_{\text{comp,isoth}} = \frac{(T_{\text{H}} - T_{\text{L}})}{T_{\text{H}}} \quad (4)$$

The formula shows that the efficiency of Carnot depends on the temperature difference between the hot and cold reservoirs, relative to the temperature of the hot reservoir.[23]

Note: *While sorption coolers have been used in previous space missions as passive or pre-cooling stages, ATHENA does not currently incorporate a sorption cooler in its baseline cryochain. Instead, it relies on a two-stage Stirling system for pre-cooling, followed by a Joule-Thomson cooler and multi-stage ADR.*

The two-stage Stirling cooler pre-cools helium gas to ~20 K, which is then transferred via heat exchangers to the JT cooler. The JT system further cools the gas to ~4 K before it enters the ADR stage. The ADR is thermally connected to the JT cold tip and activated through magnetic cycling. Thermal switches are used to isolate and engage stages during the cooldown and recycling processes.

Adiabatic Demagnetization Refrigerators (ADR):

ADRs are a type of magnetic cooler that is capable of providing milli-Kelvin cooling for space applications. To achieve cooling, the magnetization process is carried out isothermally. The heat of the magnetization is promptly removed to maintain the substance at a constant temperature. When the system is in an ordered state, it is thermally isolated, which allows an isentropic demagnetization process, where the magnetic field is gradually reduced without heat exchange, further cooling the substance. One of its unique properties is the lack of moving parts with no vibration or motion forces, making it highly reliable. There are various ADR configurations, such as cycle, two-stage, double, and continuous ADR, each suited for specific purposes.[26] For the ATHENA mission, a five-stage ADR is used, replacing earlier two-stage concepts, to provide increased cooling capacity and thermal stability.[27]

Table 1: Comparison of Cryocooler Technologies Used in ATHENA.[16,26,28,29]

Cryocooler Type	Cooling Principle	Typical Temperature Range	Moving Parts at Cold End	Vibration Level	Key Advantages	Common Use Case in ATHENA
Stirling Cooler	Regenerative cycle with pistons	~60–15 K	Yes	Moderate	High efficiency; compact	Pre-cooling for JT stage
JT Cryocooler	Isenthalpic expansion via throttling	~4 K	No	Low	No moving parts; compact; stable	Intermediate cooling before ADR
ADR	Magnetic entropy reduction via demagnetization	~50 mK	No	None	Reaches mK range; no vibrations	Final cooling for TES detectors

ATHENA Instrumentation

Cryochain at 4 K and 50 mK:

The Focal Plane Assembly (FPA) includes all the cryogenic components of the XIFU detector, positioned on the coldest part of the instrument to capture incident X-rays. These X-rays are absorbed by the detector's materials, in which their energy is measured by the Transition Edge Sensors (TES). Therefore, to optimize performance and maintain the superconducting state of the TESs, the FPA is kept at a temperature of 50 mK.[30]

To reach the desired temperature, X-IFU's cooling system relies on a multi-stage cryochain consisting of several mechanical cryocoolers, divided into upper and last-stage coolers.[31] The upper cooling chain provides cooling power at 2 K, consisting of a 15 K pulse tube, 4 K-JT, and the 2 K-JT coolers. The last stage cooler cycles at regular intervals and it cools to 50 mK, through the usage of the 300 mK sorption cooler and the ADR.[32,33]

In the cryochain, the 2 K-JT and 4 K-JT coolers are connected to a hybrid cooler using thermal straps to function as pre-coolers. However, integrating continuous cooling JT coolers into a hybrid cooler that operates in alternating phases can lead to parasitic heat flow. This unwanted heat transfer, especially during the recycling phase, can increase the thermal load on the 2 K cooler, potentially affecting its performance. Therefore, controlling parasitic heat flow can help manage the amount of heat in the JT cooler and avoid overloading. This cool-down process involves the gradual activation of the pulse tube and JT pre-coolers. As the temperature drops, the Stirling cooler provides more cooling power, ensuring a controlled and efficient method to reach its intended operating conditions.[28] The 2 K JT cooler is pre-cooled by the 15 K pulse tube coolers, while the 4 K JT is pre-cooled by the two-stage Stirling coolers. In addition, a commercial 4 K pulse tube cooler is responsible for cooling the radiative shields and the 4 K JT interface through the usage of a gas gap heat switch to control heat transfer.[29] Finally, the desired temperature of 50 mK is

DOI: 10.36838/v7i9.37

achieved through the ADR, which is connected to the 2 K stage via a heat switch. When the ADR cools to 2 K, a magnetic field is applied, which aligns the ion spins in the salt pill. This, in turn, produces heat, which is released through the heat switch until the system returns to 2 K. Once the ADR stage is insulated by opening the heat switch, the magnetic field is reduced, randomizing the paramagnetic ions once again, further lowering its temperature. The ADR's temperature is regulated by adjusting the magnetic field, which must be decreased over time to compensate for the heat loss of the system.[34]

TES Detectors:

The X-IFU system is based on an array of X-ray absorbers linked to Transition Edge Sensors (TES), which function as micro-calorimeters. The TES detects the heat pulses generated by absorbed X-ray photons, measuring the temperature variation (a 300-400 microsecond pulse) through changes in its electrical resistance. Therefore, TES needs to be cooled to temperatures below 100 mK, with the system's thermal bath set at 50 mK, maintained by an ADR and a pulse tube cryocooler. It is also adjusted to transition between superconducting and normal states for optimal sensitivity.[35] Furthermore, the main TES array is operated using frequency domain multiplexed (FDM) SQUID readout electronics, which are used to achieve low-noise, low-dissipation readout of the low-impedance TES pixels.[33]

As TES detectors are highly sensitive to mechanical vibrations, a "50 mK snout" is suspended from the refrigerators' mixing chamber using a two-stage Kevlar vibration isolation system. This minimizes lower-frequency noise that could cause power dissipation from sources such as the pulse tube cryocooler.[36]

Furthermore, a small coil is placed over the TES chip to generate a small magnetic field when a current is passed through the wire. This helps reduce any residual external magnetic field. The field coil is mounted on a mechanical support that also serves as an X-ray collimator, which ensures that only the active pixels are exposed to X-rays, reducing interference between them. This improves the accuracy and sensitivity of TES and helps detect X-rays more effectively. The shape of the resistive TES transition depends on the current, temperature, and the magnetic field. TESs are highly sensitive to both static and dynamic magnetic fields, with greater sensitivity in the direction perpendicular to the TES.[37] Therefore, the FPA features magnetic and stray light shielding, electromagnetic compatibility (EMC) shielding, and filtering. This protects TES from environmental disturbances during ground tests and in-flight operations and reaches its required performance.[33]

Science Goals

Aims 1 (Accretion Physics around Compact Objects:

The ATHENA mission is structured around three main scientific missions. The first is the physics of accretion around black holes, neutron stars, and other compact objects. The second is cosmic feedback, the process by which accretion and star formation are interconnected to the formation and evolution of galaxies. Lastly, the third mission investigates the physical nature and evolution of the large-scale structure, particularly through the study of hot baryonic matter. Furthermore, ATHENA will also provide a major contribution to our understanding of the nature and influences of hot cosmic plasmas in all astrophysical objects, through spatially resolved high-resolution X-ray spectroscopy and sensitive wide-field X-ray imaging.[38]

Some of the most extreme physical conditions in the Universe are found in and around compact objects. For instance, black holes create the strongest gravitational fields, while neutron stars are the densest observable form of matter. Matter trapped in these extreme gravitational conditions is spun and heated, causing it to radiate X-rays. X-ray observations can measure the physical conditions in the innermost regions around black holes and neutron stars, revealing how the laws of general relativity apply under extreme circumstances and how matter behaves under such intense pressure and density. Furthermore, X-ray observations can also explore the process of accretion, where they will investigate how matter accretes into compact objects by mapping the innermost flows around black holes and measuring their spins.[38]

According to the "no hair" theorem, astrophysical black holes are characterized by two main parameters: mass and spin. However, its effects are only evident in the very innermost regions, specifically through X-ray emissions. Black hole spins are an important energy source in astrophysics as they could serve as an energy source, affecting various phenomena such as the behavior of Active Galactic Nuclei (AGNs), the powering of jets, and the production of gravitational waves when black holes are being merged. Unlike measurements of black hole mass, spin measurements can also reveal information on stellar evolution and the histories of galaxy mergers. Therefore, ATHENA will measure black hole spins of many bright Galactic Black Holes (GBHs) and AGNs, allowing the studies of fainter AGNs, which are linked to the evolution of supermassive black holes (SMBHs) and their host galaxies.[38]

Aims 2 (AGN Feedback and Galaxy Evolution):

Energy injections from growing SMBHs, known as AGN feedback, are key to understanding the formation and evolution of galaxies. This feedback can heat or expel cold gas from galaxies, driving a "downsizing" effect, in which massive galaxies form first, followed by smaller ones.[39] AGNs play a crucial role in the evolution of galaxies, where AGNs can contribute significantly due to their ability to penetrate denser gas with X-rays. Despite its significant impact on galaxy evolution models, the underlying physical processes behind its feedback are still unclear. Therefore, the ATHENA mission aims to tackle these gaps through high spectral and spatial resolution instruments to study AGN activity in galaxies and their relationship between key galaxy properties such as stellar mass, gas mass, and star-formation rates, revolutionizing our understanding of early SMBHs and their impact on galaxy evolution.[39]

DOI: 10.36838/v7i9.37

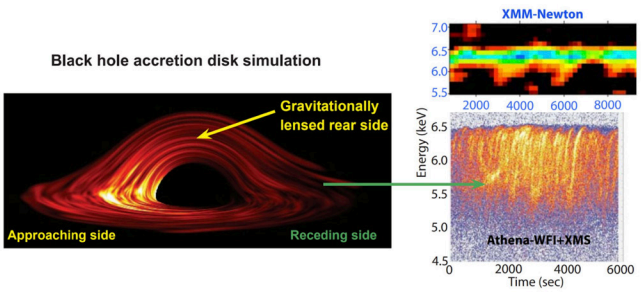

Figure 3: Left: Snapshot from a time-dependent Magneto-Hydrodynamic (MHD) simulation of an accretion disk around a BH (Armitage & Reynolds 2003). Rings and hotspots of emission are seen due to turbulence, the emission from which should be modulated on the orbital timescale. Right: Because the features are variable in both flux and energy, the disk can be mapped out in the time-energy plane. The first hints of this behavior have been seen in XMM-Newton data (Iwasawa *et al.* 2004; upper right), but the factor ~ 4 improvement in throughput and ~ 40 in energy resolution offered by Athena are needed to sample weaker and (possibly) narrower features on suborbital timescales, allowing us to map out the inner accretion flow. Only unusually strong and slow flares can be detected by XMM-Newton. (Reference numbers have been modified from the original source.)[38] Figure 3 presents a snapshot from a magneto-hydrodynamic (MHD) simulation, showing turbulent gas flows and variability in density and velocity. It reflects the dynamic environments Athena aims to observe with high time-energy resolution.

Reverberation mapping is a technique used to study the inner accretion flows by measuring the light travel time it takes for X-ray light to affect the emission lines produced in the accretion disk. The ATHENA will observe matter within a few gravitational radii of the event horizon of black holes. Under these extreme environments, large gravitational redshifts, extreme light bending, and time delay effects will cause spectral and timing signatures in X-ray emission, which can reveal the black hole's spin and the effects of gravity near the black hole.[38] X-rays provide a unique opportunity to study the innermost regions around SMBHs in AGNs. Therefore, the X-IFU of the ATHENA mission can provide precise measurements of black hole spins and properties of AGN outflows through its unprecedented sensitivity.[40] As illustrated in Figure 4, reverberation mapping provides insight into the structure near black holes by measuring time lags in X-ray emission.

Aims 3 (Large-Scale Structure and Baryonic Matter):

Large-scale structures are the largest arrangement of matter in the universe, which are shaped by gravity over billions of years. These structures grow over cosmic time through the accretion of gas from the intergalactic medium, which constitutes the majority of the baryonic matter in the local universe. Tracing the physical evolution of galaxy clusters and groups from their formation epoch to the present day can reveal insights into their formation and evolution.[41] However, the majority of the hot baryons are not in clusters, and their location and physical states are currently unknown. More than 30 percent of the baryons in today's universe are expected to reside in the Warm/Hot Intergalactic Medium (WHIM), a region in the universe filled with warm and hot gas. Baryons align with the filamentary structure of dark matter, thus, their location is influenced by the distribution of dark matter. Therefore, determining baryonic matter requires detecting resonance absorption lines, which occur when x-rays from a bright background source pass through hot diffuse plasma,[42] revealing its composition, properties, and origin.[41]

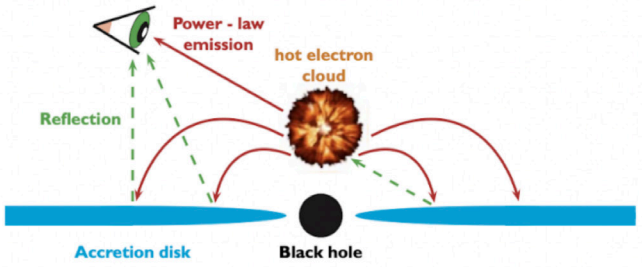

Figure 4: Cartoon of a black hole and accretion disk (blue) above which the power-law continuum is generated by Comptonisation of thermal disk photons in a hot electron cloud (orange). Power-law emission (red) irradiates the disk, producing the reflection spectrum (green). Intrinsic variations in the power-law source create delayed, blurred changes (reverberation) in reflection. Thanks to Athena, it will be possible to translate these signals into a physical picture of the inner region around the black hole. The reflection features and thermal disk emission both provide an independent estimate of the inner accretion disk radius via the maximum gravitational redshift of emission features and the disk temperature. (Reference numbers have been modified from the original source.)[38] Figure 4 visualizes how X-ray echoes from the accretion disk are used to map structures close to a black hole. The time lag between direct and reflected X-rays provides information about the disk's geometry and inner radius.

The universe contains large amounts of hot gas, which exists at extremely high temperatures. On the largest scales, clusters of galaxies form in regions where dark matter created the deepest potential wells, which are regions with strong gravitational pull. These wells trap the hot gas, which causes it to accumulate within the clusters, which are in a state of hydrostatic equilibrium. Hydrostatic equilibrium is when the pressure of the hot gas balances the gravitational pull of the cluster, preventing it from collapsing further. Therefore, how baryons are pulled into these clusters and how they evolve gives insight into the cosmological evolution of the universe.[42] X-ray observations can reveal information on the velocities, thermodynamics, and chemical composition of the gas, which can provide insight into how baryons evolve inside the gravitational potential wells of galaxy clusters.[43]

Supersonic events release huge amounts of energy and elements, impacting the interstellar medium through heating, turbulence, heavy element enrichment, particle acceleration, and magnetic field amplification. X-ray emissions from hot plasma offer key insights into its compositions and processes, such as its ionization states.[44] Heavy elements produced in stellar processes, such as oxygen, neon, magnesium, silicon, sulfur, argon, calcium, and iron, are crucial to understanding the chemical evolution of the universe. The X-IFU would be able to observe these elements and create maps of metal distribution in clusters. These maps will cover unprecedented distances, showing how metals are distributed in the entire cluster volume.[41]

DOI: 10.36838/v7i9.37

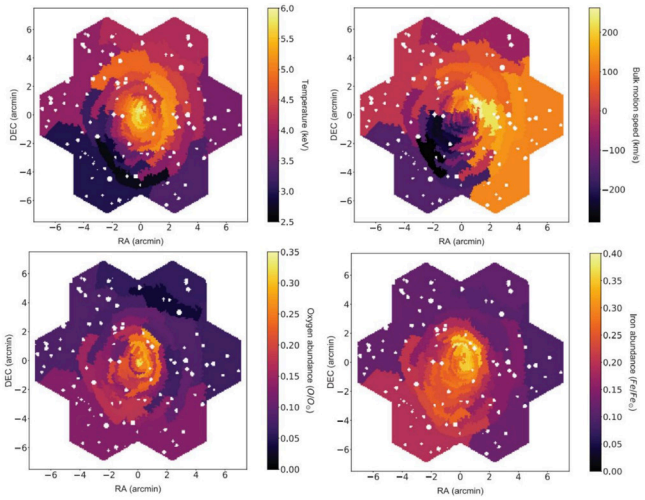

Figure 5: Physical parameter maps reconstructed from seven 100-ks X-IFU observations of a galaxy cluster over regions of S/N 300 (90,000 counts), simulated using the instrument end-to-end simulator SIXTE (Dauser *et* al. 2019). The cluster is located at z = 0.1, with R500 = 1.1 Mpc, and T500 = 4.2 keV. Input clusters are taken from large-scale hydrodynamic simulations performed using the GADGET-3 smoothed-particle hydrodynamics code· (From top left to bottom right) Spectral-like temperature (keV), bulk velocity deduced from line-shift with respect to the cluster's average redshift (km/s), and emission-measure-weighted oxygen and iron abundance (with respect to solar). The image is taken from (Cucchetti *et al.* 2018), and references therein. White holes in the maps are associated with subtracted point sources. (Reference numbers have been modified from the original source.)[44] Reconstructed parameter maps reveal temperature, metallicity, and velocity variations within a simulated galaxy cluster. Figure 5 demonstrates Athena's capability to spatially resolve complex intracluster medium dynamics.

The ATHENA mission would provide the necessary angular resolution, spectral resolution, throughput, detection sensitivity, and survey grasp to revolutionize our understanding of these issues. With X-IFU's spatially resolved high-resolution X-ray spectroscopy and the WIFI's wide field X-ray imaging, ATHENA would be able to map the outskirts of nearby galaxy clusters in detail. These observations will measure the emission, temperature, and metallicity of the ICM. This will reveal the physical state of the accreted material, leading to a comprehensive understanding of how galaxy structures assemble and grow over time.[41] Specifically, ATHENA will use the X-IFU to reveal the location, chemical composition, physical state, and dynamics of baryons in the local universe, focusing specifically on the Warm-Hot Intergalactic Medium (WHIM). This can be achieved through nominal resolution, where gamma-ray bursts afterglows are used as background sources shining through the cosmic web.[44] Thus, the ATHENA mission would be able to study how baryonic gas accretes and evolves in the dark matter potential wells by measuring motions and turbulence in the ICM.

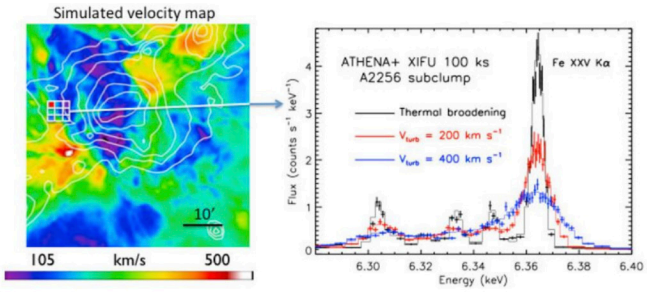

Figure 6: Athena+ X-IFU spectrum of a subclump in the galaxy cluster A2256, demonstrating the high precision measurements possible for the ICM velocity field. Left: Velocity map of a cosmological hydrodynamical simulation of a perturbed galaxy cluster of about M200 ~ 1015M⊙ with X-ray surface brightness contours overlaid. Right: Simulated spectrum for a 100 ks observation with Athena+ XIFU for a 1.5 arcmin region (one of the 9 small regions shown on the image), showing the turbulent broadening of the Fe XXV Kα line. Simulated data with vturb = 200 km s−1 are shown in red· Black and blue represent the model with vturb = 0 and vturb = 400 km s−1, respectively. For an input turbulent velocity of 0, 200, 400 km s−1, the 1σ statistical uncertainty is ±20, ±5, and ±10 km s−1, respectively. (Reference numbers have been modified from the original source.)[41]

Figure 6 shows simulated spectral data distinguishing chemical elements and physical conditions across a supernova remnant. It highlights Athena's ability to dissect remnants at high spatial and spectral resolution.

Discussion

The multi-stage cryochain for ATHENA demonstrates how combining Stirling coolers, Joule-Thomson systems, and Adiabatic Demagnetization Refrigerators successfully achieves the 50 mK temperatures required for high-resolution X-ray spectroscopy. This cooling system represents an engineering achievement that directly enables ATHENA's scientific capabilities. For instance, cryogenically cooled TES detectors onboard Hitomi enabled the most precise measurement to date of turbulent motion in the Perseus galaxy cluster's hot gas45 — a discovery that reshaped models of how energy spreads in large-scale structures. The selection of appropriate cryocoolers involves balancing cooling capacity with reliability, compactness, vibration control, and longevity—all critical factors for space applications where maintenance is impossible. Each technology contributes distinct advantages: Stirling coolers provide reliable medium-temperature cooling, JT coolers offer stability without moving parts at the cold end, and ADRs achieve the final cooling step with minimal vibration.

ATHENA's cryogenic technologies represent a substantial improvement over previous X-ray missions, with approximately 40 times better energy resolution than XMM-Newton. This advancement will revolutionize our understanding of cosmic phenomena from black hole physics to the formation of large-scale structures. The relationship between cryogenic engineering and astronomical discovery highlights how technological innovation directly enables scientific breakthroughs in space exploration.

All figures used in this paper are either original or adapted from publicly available ESA documentation and related scientific publications. Proper attribution has been maintained wherever applicable.

Conclusions

The ATHENA mission represents a significant advancement in X-ray astronomy, made possible through innovative cryogenic cooling technologies. This study has demonstrated how the multi-stage cryochain—combining Stirling coolers, Joule-Thomson systems, and Adiabatic Demagnetization Refrigerators—enables the X-IFU instrument to achieve the ultra-low temperatures of 50 mK required for high-resolution spectroscopy.

The selection of appropriate cryocoolers for space applications involves careful consideration of cooling power, reliability, compactness, vibration control, and longevity. Each cryocooler type offers distinct advantages: Stirling coolers provide reliability and efficiency for medium-low temperatures; Joule-Thomson coolers offer stability and compact design for reaching liquid helium temperatures; and ADRs enable the achievement of milli-Kelvin temperatures with minimal vibration.

The Transition Edge Sensors at the core of the X-IFU detector system demonstrate how these cooling technologies directly enable scientific discovery. By operating at 50 mK, these sensors achieve the exceptional energy resolution needed to study the physics of black holes, cosmic feedback mechanisms, and the formation of large-scale cosmic structures.

This research highlights the critical relationship between advanced cooling technologies and breakthrough astronomical observations. By pushing the boundaries of cryogenic engineering, ATHENA will provide unprecedented insights into the hot and energetic universe, revolutionizing our understanding of cosmic phenomena from black hole physics to galaxy evolution and large-scale structure formation.

References

1. Barcons, X., Nandra, K., Barret, D., Herder, J.-W., Fabian, A.C., Piro, L., Watson, M.G., Athena team: Athena: the x-ray observatory to study the hot and energetic universe. Journal of Physics: Conference Series 610(1), 012008 (2015) https://doi.org/10.1088/1742-6596/610/1/012008
2. N., R., Martin, D., Lumb, D., Verhoeve, P., Oosterbroek, T., Bavdaz, M., Fransen, S., Linder, M., Peyrou-Lauga, R., Voirin, T., Braghin, M., Mangunsong, S., Pelt, M., Wille, E.: Status of the esa l1 mission candidate Athena. In: Takahashi, T., Murray, S.S., den Herder, J.-W.A. (eds.) Space Telescopes and Instrumentation 2012: Ultraviolet to Gamma Ray. Society of Photo-Optical Instrumentation Engineers (SPIE) Conference Series, vol. 8443, p. 844328 (2012). https://doi.org/10.1117/12.924820
3. Barret, D., Albouys, V., Herder, J.-W.d., Piro, L., Cappi, M., Huovelin, J., Kelley, R., Mas-Hesse, J.M., Paltani, S., Rauw, G., Rozanska, A., Svoboda, J., Wilms, J., Yamasaki, N., Audard, M., Bandler, S., Barbera, M., Barcons, X., Bozzo, E., Ceballos, M.T., Charles, I., Costantini, E., Dauser, T., Decourchelle, A., Duband, L., Duval, J.-M., Fiore, F., Gatti, F., Goldwurm, A., Hartog, R.d., Jackson, B., Jonker, P., Kilbourne, C., Korpela, S., Macculi, C., Mendez, M., Mitsuda, K., Molendi, S., Pajot, F., Pointecouteau, E., Porter, F., Pratt, G.W., Prˆele, D., Ravera, L., Sato, K., Schaye, J., Shinozaki, K., Skup, K., Soucek, J., Thibert, T., Vink, J., Webb, N., Chaoul, L., Raulin, D., Simionescu, A., Torrejon, J.M., Acero, F., Branduardi-Raymont, G., Ettori, S., Finoguenov, A., Grosso, N., Kaastra, J., Mazzotta, P., Miller, J., Miniutti, G., Nicastro, F., Sciortino, S., Yamaguchi, H., Beaumont, S., Cucchetti, E., D'Andrea, M., Eckart, M., Ferrando, P., Kammoun, E., Lotti, S., Mesnager, J.-M., Natalucci, L., Peille, P., Plaa, J., Ardellier, F., Argan, A., Bellouard, E., Carron, J., Cavazzuti, E., Fiorini, M., Khosropanah, P., Martin, S., Perry, J., Pinsard, F., Pradines, A., Rigano, M., Roelfsema, P., Schwander, D., Torrioli, G., Ullom, J., Vera, I., Villegas, E.M., Zuchniak, M., Brachet, F., Cicero, U.L., Doriese, W., Durkin, M., Fioretti, V., Geoffray, H., Jacques, L., Kirsch, C., Smith, S., Adams, J., Gloaguen, E., Hoogeveen, R., Hulst, P., Kiviranta, M., Kuur, J., Ledot, A., Leeuwen, B.-J., Loon, D., Lyautey, B., Parot, Y., Sakai, K., Weers, H., Abdoelkariem, S., Adam, T., Adami, C., Aicardi, C., Akamatsu, H., Alonso, P.E.M., Amato, R., Andr´e, J., Angelinelli, M., Anon-Cancela, M., Anvar, S., Atienza, R., Attard, A., Auricchio, N., Balado, A., Bancel, F., Barusso, L.F., Bascu˜nan, A., Bernard, V., Berrocal, A., Blin, S., Bonino, D., Bonnet, F., Bonny, P., Boorman, P., Boreux, C., Bounab, A., Boutelier, M., Boyce, K., Brienza, D., Bruijn, M., Bulgarelli, A., Calarco, S., Callanan, P., Campello, A.P., Camus, T., Canourgues, F., Capobianco, V., Cardiel, N., Castellani, F., Cheatom, O., Chervenak, J., Chiarello, F., Clerc, L., Clerc, N., Cobo, B., CoeurJoly, O., Coleiro, A., Colonges, S., Corcione, L., Coriat, M., Coynel, A., Cuttaia, F., D'Ai, A., D'anca, F., Dadina, M., Daniel, C., Dauner, L., DeNigris, N., Dercksen, J., DiPirro, M., Doumayrou, E., Dubbeldam, L., Dupieux, M., Dupourqu´e, S., Durand, J.L., Eckert, D., Eiriz, V., Ercolani, E., Etcheverry, C., Finkbeiner, F., Fiocchi, M., Fossecave, H., Franssen, P., Frericks, M., Gabici, S., Gant, F., Gao, J.-R., Gastaldello, F., Genolet, L., Ghizzardi, S., Gil, M.A.A., Giovannini, E., Godet, O., Gomez-Elvira, J., Gonzalez, R., Gonzalez, M., Gottardi, L., Granat, D., Gros, M., Guignard, N., Hieltjes, P., Hurtado, A.J., Irwin, K., Jacquey, C., Janiuk, A., Jaubert, J., Jim´enez, M., Jolly, A., Jourdan, T., Julien, S., Kedziora, B., Korb, A., Kreykenbohm, I., K¨onig, O., Langer, M., Laudet, P., Laurent, P., Laurenza, M., Lesrel, J., Ligori, S., Lorenz, M., Luminari, A., Maffei, B., Maisonnave, O., Marelli, L., Massonet, D., Maussang, I., Melchor, A.G., Le Mer, I., Millan, F.J.S., Millerioux, J.-P., Mineo, T., Minervini, G., Molin, A., Monestes, D., Montinaro, N., Mot, B., Murat, D., Nagayoshi, K., Naz´e, Y., Nogu`es, L., Pailot, D., Panessa, F., Parodi, L., Petit, P., Piconcelli, E., Pinto, C., Plaza, J.M.E., Plaza, B., Poyatos, D., Prouv´e, T., Ptak, A., Puccetti, S., Puccio, E., Ramon, P., Reina, M., Rioland, G., Rodriguez, L., Roig, A., Rollet, B., Roncarelli, M., Roudil, G., Rudnicki, T., Sanisidro, J., Sciortino, L., Silva, V., Sordet, M., Soto-Aguilar, J., Spizzi, P., Surace, C., S´anchez, M.F., Taralli, E., Terrasa, G., Terrier, R., Todaro, M., Ubertini, P., Uslenghi, M., Vaate, J.G.B., Vaccaro, D., Varisco, S., Varni`ere, P., Vibert, L., Vidriales, M., Villa, F., Vodopivec, B.M., Volpe, A., Vries, C., Wakeham, N., Walmsley, G., Wise, M., Wit, M., Wo´zniak, G.: The athena x-ray integral field unit: a consolidated design for the system requirement review of the preliminary definition phase. Experimental Astronomy 55(2), 373–426 (2023) https://doi.org/10.1007/s10686-022-09880-7
4. Kammoun, E. S., Barret, D., Peille, P., Willingale, R., Dauser, T., Wilms, J., Guainazzi, M., Miller, J. M.: The defocused observations of bright sources with athena/x-ifu. A & A 664, 29 (2022) https://doi.org/10.1051/0004-6361/202243606
5. Barret, D., Trong, T.L., Herder, J.-W., et al. (2018). The Athena X-ray Integral Field Unit (X-IFU). In: Space Telescopes and Instrumentation 2018: Ultraviolet to Gamma Ray, Proc. SPIE 10699, 106991G. https://doi.org/10.1117/12.2312409
6. Chan, C.K., Tward, E., Burt, W.W.: In: Fast, R.W. (ed.) Overview of Cryocooler Technologies for Space-Based Electronics and Sensors, pp. 1239–1250. Springer, Boston, MA (1990). https://doi.org/10.1007/978-1-4613-0639-9148
7. Radebaugh, R.: Cryocoolers: the state of the art and recent developments. Journal of Physics: Condensed Matter 21(16) (2009) https://doi.org/10.1088/0953-8984/21/16/164219

DOI: 10.36838/v7i9.37

8. Standards, N.I., Technology: Cryocoolers. https://trc.nist.gov/cryogenics/ cryocoolers.html. Accessed: 2024-07-22
9. Gilmore, D.G.: Spacecraft Thermal Control Handbook: Cryogenics. Spacecraft Thermal Control Handbook Volume II – Cryogenics. The Aerospace Press / AIAA (2002). https://books.google.co.kr/books?id=fshGaOLiuFgC
10. Zagarola, M.V., Breedlove, J.F., McCormick, J.A., Swift, W.L.: Turbo-Brayton cryocooler technology for low-temperature space applications. In: Mather, J.C. (ed.) IR Space Telescopes and Instruments, vol. 4850, pp. 1029–1037. SPIE, 4850 (2003). International Society for Optics and Photonics. https://doi.org/10.1117/12.461776
11. Rana, H.: Advancing cryogenic systems for the next generation of astrophysics discoveries. IAF Technical Papers 74 (2023)
12. de Waele, A.T.A.M.: Pulse-tube refrigerators: principle, recent developments, and prospects. Physica B: Condensed Matter 280(1), 479–482 (2000) https://doi.org/10.1016/S0921-4526(99)01840-2
13. Rana, H., Akiyama, K., Canavan, E., DiPirro, M., Freeman, M., Galison, P., Grimes, P., Honma, M., Houston, J., Johnson, M., Kimball, M., Marrone, D., Tong, E.: The Black Hole Explorer Cryocooling Instrument (2024). https://arxiv.org/abs/2406.09975
14. Kittel, P., Feller, J., Roach, P., Kashani, A., Helvensteijn, B.: Cryocoolers for space. ResearchGate (2004)
15. Department of Engineering Science, University of Oxford: Cryocoolers for Space Applications. https://eng.ox.ac.uk/cryogenics/research/ cryocoolers-for-space-applications/. Accessed: 2024-07-23
16. Chen, W.: Performance characteristics comparison of major types of mechanical cryocoolers for aerospace applications. IOP Conference Series: Materials Science and Engineering 755, 012007 (2020) https://doi.org/10.1088/1757-899X/755/1/012007
17. Rawlings, T.: Numerical modeling of Stirling cryocoolers. PhD thesis, University College London (February 2022)
18. Maldonado Aguilar Diego Jos´e, Au˜n´on Hidalgo, Juan Antonio, Eskubi, Mauri, Mart´ınez, Pablo: Analysis of the operating parameters in a Stirling cryocooler. E3S Web Conf. 313, 10002 (2021) https://doi.org/10.1051/e3sconf/202131310002
19. Abolghasemi, M.A., Rana, H., Stone, R., Dadd, M., Bailey, P., Liang, K.: Coaxial Stirling pulse tube cryocooler with active displacer. Cryogenics 111, 103143 (2020) https://doi.org/10.1016/j.cryogenics.2020.103143
20. Radebaugh, R.: Thermodynamics of Regenerative Refrigerators. Thermodynamics of Tegenerative Refrigerators Book Chapter: Generation of Low Temperature and its Applications., https://doi.org/10.1007/978-0-387-71752-4_4 (2008)
21. Pan, X., Liu, S., Wu, Y., Jiang, Z., Ding, L.: Development of a 2-4 k closed-cycle jt cryocooler for space application. IOP Conference Series: Materials Science and Engineering 1240(1), 012016 (2022) https://doi.org/10.1088/1757-899X/1240/1/012016
22. Singh, A., Singh, P.: CFD analysis of Stirling cryocoolers. Master's thesis, National Institute of Technology Rourkela (2012)
23. Tarish, A.P.D.A., Alwan, N., Ali, B., Ali, O., Aslan, S., Alomar, O.: Design and performance analysis of Joule-Thomson cryocooler systems. Energy Reports 11, 4572–4586 (2024) https://doi.org/10.1016/j.egyr.2024.04.034
24. Ardhapurkar, P.M., Atrey, M.D.: Performance optimization of a miniature Joule–Thomson cryocooler using numerical model. Cryogenics 63, 94–101 (2014) https://doi.org/10.1016/j.cryogenics.2014.07.006
25. Waele, A.: Basics of Joule–Thomson liquefaction and jt cooling. Journal of Low Temperature Physics 186 (2017) https://doi.org/10.1007/s10909-016-1733-3
26. Weatherstone, S.A.: Development of milli-kelvin adr technology for space missions. PhD thesis, University College London (2012)
27. Jin, H., Shen, J., Li, C.Z., Wang, C., Yu, F.Q., Zu, H.Y., Liu, P., Ding, J., Li, K., Wang, Y.N., Dai, W., Zhou, Y., Cui, W.: Development of adiabatic demagnetization refrigerator for future astronomy missions. IOP Conference Series: Materials Science and Engineering 1240(1), 012027 (2022) https://doi.org/10.1088/1757-899X/1240/1/012027
28. Prouvé, T., Duval, J.M., Charles, I., et al. (2018). Athena X-IFU 300K–50 mK cryochain demonstrator cryostat. Cryogenics 89, 85–94. https://doi.org/10.1016/j.cryogenics.2017.11.009
29. Shinozaki, K., Tokoku, C., Yamamoto, R., *et al.* (2019). Cooling performance of Joule-Thomson coolers in 300 K–50 mK cryochain demonstration for Athena X-IFU. IOP Conf. Ser.: Mater. Sci. Eng. 502, 012069. https://doi.org/10.1088/1757-899X/502/1/012069
30. Betancourt-Martinez, G.L., Pajot, F., Roudil, G., Adams, J., Bandler, S., Beaumont, S., Bertrand, B., Castellani, F., Cucchetti, E., Dupieux, M., Geoffray, H., Peille, P., Ravera, L., Wernicke, D., Ledot, A.: A test platform for the detection and readout chain for the Athena X-IFU. In: Herder, J.-W.A., Nakazawa, K., Nikzad, S. (eds.) Space Telescopes and Instrumentation 2020: Ultraviolet to Gamma Ray, vol. 10699, p. 55. SPIE, San Diego, CA (2021). SPIE
31. Barret, D., Herder, J.W., Piro, L., Ravera, L., Hartog, R.D., Macculi, C., Barcons, X., Page, M., Paltani, S., Rauw, G., Wilms, J., Ceballos, M., Duband, L., Gottardi, L., Lotti, S., Plaa, J., Pointecouteau, E., Schmid, C., Akamatsu, H., Bagliani, D., Bandler, S., Barbera, M., Bastia, P., Biasotti, M., Branco, M., Camon, A., Cara, C., Cobo, B., Colasanti, L., Costa-Kramer, J.L., Corcione, L., Doriese, W., Duval, J.M., Fabrega, L., Gatti, F., Gerone, M., Guttridge, P., Kelley, R., Kilbourne, C., Kuur, J., Mineo, T., Mitsuda, K., Natalucci, L., Ohashi, T., Peille, P., Perinati, E., Pigot, C., Pizzigoni, G., Pobes, C., Porter, F., Renotte, E., Sauvageot, J.L., Sciortino, S., Torrioli, G., Valenziano, L., Willingale, D., Vries, C., Weers, H.: The Hot and Energetic Universe: The X-ray Integral Field Unit (X-IFU) for Athena+ (2013). https://arxiv.org/abs/1308.6784
32. Pajot, F., Barret, D., Lam-Trong, T., Herder, J.-W., Piro, L., Cappi, M., Huovelin, J., Kelley, R., Mas-Hesse, J.M., Mitsuda, K., Paltani, S., Rauw, G., Rozanska, A., Wilms, J., Barbera, M., Douchin, F., Geoffrey, H., Hartog, R., Kilbourne, C., Du, M.L., Macculi, C., Mesnager, J.-M., Peill, P.: The Athena x-ray integral field unit (x-ifu). Journal of Low Temperature (2018)
33. Barret, D., Lam Trong, T., Herder, J.-W., Piro, L., Barcons, X., Huovelin, J., Kelley, R., Mas-Hesse, J.M., Mitsuda, K., Paltani, S., Rauw, G., Ro˙zanska, A., Wilms, J., Barbera, M., Bozzo, E., Ceballos, M.T., Charles, I., Decourchelle, A., Hartog, R., Duval, J.-M., Fiore, F., Gatti, F., Goldwurm, A., Jackson, B., Jonker, P., Kilbourne, C., Macculi, C., Mendez, M., Molendi, S., Orleanski, P., Pajot, F., Pointecouteau, E., Porter, F., Pratt, G.W., Prˆele, D., Ravera, L., Renotte, E., Schaye, J., Shinozaki, K., Valenziano, L., Vink, J., Webb, N., Yamasaki, N., Delcelier-Douchin, F., Le Du, M., Mesnager, J.-M., Pradines, A., BranduardiRaymont, G., Dadina, M., Finoguenov, A., Fukazawa, Y., Janiuk, A., Miller, J., Naz´e, Y., Nicastro, F., Sciortino, S., Torrejon, J.M., Geoffray, H., Hernandez, I., Luno, L., Peille, P., Andr´e, J., Daniel, C., Etcheverry, C., Gloaguen, E., Hassin, J., Hervet, G., Maussang, I., Moueza, J., Paillet, A., Vella, B., Campos Garrido, G., Damery, J.-C., Panem, C., Panh, J., Bandler, S., Biffi, J.-M., Boyce, K., Cl´enet, A., DiPirro, M., Jamotton, P., Lotti, S., Schwander, D.,Smith, S., Leeuwen, B.-J., Weers, H., Brand, T., Cobo, B., Dauser, T., Plaa, J., Cucchetti, E.: The athena x-ray integral field unit (x-ifu). In:

Herder, J.-W.A., Takahashi, T., Bautz, M. (eds.) Space Telescopes and Instrumentation 2016: Ultraviolet to Gamma Ray, 99052F (17 August 2016); https://doi.org/10.1117/12.2232432
34. Beaumont, S. (2023). High-resolution X-ray spectroscopy with the Athena/X-IFU: Microcalorimeters development and feasibility studies. PhD thesis, Université Paul Sabatier – Toulouse III. https://theses.hal.science/tel-04192223
35. Corcione, L., Ligori, S., Capobianco, V., *et al*. (2016). Conceptual design of the X-IFU Instrument Control Unit on board the ESA Athena mission. In: Space Telescopes and Instrumentation 2016: Ultraviolet to Gamma Ray, Proc. SPIE 9905, 990562. https://doi.org/10.1117/12.2234211
36. Vaccaro, D., Kuur, J., Hulst, P., *et al*. (2024). System performance of a cryogenic test-bed for the time-division multiplexing readout for NewAthena X-IFU. arXiv:2409.05643. https://arxiv.org/abs/2409.05643
37. Betancourt-Martinez, G., Pajot, F., Beaumont, S., *et al*. (2021). A test platform for the detection and readout chain for the Athena X-IFU. arXiv:2107.03412. https://doi.org/10.48550/arXiv.2107.03412
38. Barcons, X., Barret, D., Decourchelle, A., Herder, J.-W., Dotani, T., Fabian, A.C., *et al*. (2012). Athena (Advanced Telescope for High ENergy Astrophysics) Assessment Study Report for ESA Cosmic Vision 2015–2025. arXiv:1207.2745. https://arxiv.org/abs/1207.2745
39. Aird, J., Comastri, A., Brusa, M., *et al.* (2013). The Hot and Energetic Universe: The formation and growth of the earliest supermassive black holes. arXiv:1306.2325. https://arxiv.org/abs/1306.2325
40. Barret, D., Cappi, M. (2019). Inferring black hole spins and probing accretion/ejection flows in AGNs with the Athena X-ray Integral Field Unit. A&A 628, A5. https://doi.org/10.1051/0004-6361/201935817
41. Nandra, K., Barret, D., Barcons, X., Fabian, A., Herder, J.-W., Piro, L., Watson, M., Adami, C., Aird, J., Afonso, J.M., Alexander, D., Argiroffi, C., Amati, L., Arnaud, M., Atteia, J.-L., Audard, M., Badenes, C., Ballet, J., Ballo, L., Bamba, A., Bhardwaj, A., Battistelli, E.S., Becker, W., Becker, M.D., Behar, E., Bianchi, S., Biffi, V., Bˆırzan, L., Bocchino, F., Bogdanov, S., Boirin, L., Boller, T., Borgani, S., Borm, K., Bouch´e, N., Bourdin, H., Bower, R., Braito, V., Branchini, E., Branduardi-Raymont, G., Bregman, J., Brenneman, L., Brightman, M., Br¨uggen, M., Buchner, J., Bulbul, E., Brusa, M., Bursa, M., Caccianiga, A., Cackett, E., Campana, S., Cappelluti, N., Cappi, M., Carrera, F., Ceballos, M., Christensen, F., Chu, Y.-H., Churazov, E., Clerc, N., Corbel, S., Corral, A., Comastri, A., Costantini, E., Croston, J., Dadina, M., D'Ai, A., Decourchelle, A., Ceca, R.D., Dennerl, K., Dolag, K., Done, C., Dovciak, M., Drake, J., Eckert, D., Edge, A., Ettori, S., Ezoe, Y., Feigelson, E., Fender, R., Feruglio, C., Finoguenov, A., Fiore, F., Galeazzi, M., Gallagher, S., Gandhi, P., Gaspari, M., Gastaldello, F., Georgakakis, A., Georgantopoulos, I., Gilfanov, M., Gitti, M., Gladstone, R., Goosmann, R., Gosset, E., Grosso, N., Guedel, M., Guerrero, M., Haberl, F., Hardcastle, M., Heinz, S., Herrero, A.A., Herv´e, A., Holmstrom, M., Iwasawa, K., Jonker, P., Kaastra, J., Kara, E., Karas, V., Kastner, J., King, A., Kosenko, D., Koutroumpa, D., Kraft, R., Kreykenbohm, I., Lallement, R., Lanzuisi, G., Lee, J., Lemoine-Goumard, M., Lobban, A., Lodato, G., Lovisari, L., Lotti, S., McCharthy, I., McNamara, B., Maggio, A., Maiolino, R., Marco, B.D., Martino, D., Mateos, S., Matt, G., Maughan, B., Mazzotta, P., Mendez, M., Merloni, A., Micela, G., Miceli, M., Mignani, R., Miller, J., Miniutti, G., Molendi, S., Montez, R., Moretti, A., Motch, C., Naz´e, Y., Nevalainen, J., Nicastro, F., Nulsen, P., Ohashi, T., O'Brien, P., Osborne, J., Oskinova, L., Pacaud, F., Paerels, F., Page, M., Papadakis, I., Pareschi, G., Petre, R., Petrucci, P.-O., Piconcelli, E., Pillitteri, I., Pinto, C., Plaa, J., Pointecouteau, E., Ponman, T., Ponti, G., Porquet, D., Pounds, K., Pratt, G., Predehl, P., Proga, D., Psaltis, D., Rafferty, D., Ramos-Ceja, M., Ranalli, P., Rasia, E., Rau, A., Rauw, G., Rea, N., Read, A., Reeves, J., Reiprich, T., Renaud, M., Reynolds, C., Risaliti, G., Rodriguez, J., Hidalgo, P.R., Roncarelli, M., Rosario, D., Rossetti, M., Rozanska, A., Rovilos, E., Salvaterra, R., Salvato, M., Salvo, T.D., Sanders, J., Sanz-Forcada, J., Schawinski, K., Schaye, J., Schwope, A., Sciortino, S., Severgnini, P., Shankar, F., Sijacki, D., Sim, S., Schmid, C., Smith, R., Steiner, A., Stelzer, B., Stewart, G., Strohmayer, T., Str¨uder, L., Sun, M., Takei, Y., Tatischeff, V., Tiengo, A., Tombesi, F., Trinchieri, G., Tsuru, T.G., Ud-Doula, A., Ursino, E., Valencic, L., Vanzella, E., Vaughan, S., Vignali, C., Vink, J., Vito, F., Volonteri, M., Wang, D., Webb, N., Willingale, R., Wilms, J., Wise, M., Worrall, D., Young, A., Zampieri, L., Zand, J.I., Zane, S., Zezas, A., Zhang, Y., Zhuravleva, I.: The Hot and Energetic Universe: A White Paper presenting the science theme motivating the Athena+ mission (2013). https://arxiv.org/abs/1306.2307
42. Barcons, X., Nandra, K., Barret, D., Herder, J.-W., Fabian, A.C., Piro, L., Watson, M.G., Athena team: Athena: the x-ray observatory to study the hot and energetic universe. Journal of Physics: Conference Series 610(1), 012008 (2015) https://doi.org/10.1088/1742-6596/610/1/012008
43. Barret, D., Nandra, K., Barcons, X., Fabian, A., Herder, J.-W., Piro, L., Watson, M., Aird, J., Branduardi-Raymont, G., Cappi, M., Carrera, F., Comastri, A., Costantini, E., Croston, J., Decourchelle, A., Done, C., Dovciak, M., Ettori, S., Finoguenov, A., Georgakakis, A., Jonker, P., Kaastra, J., Matt, G., Motch, C., O'Brien, P., Pareschi, G., Pointecouteau, E., Pratt, G., Rauw, G., Reiprich, T., Sanders, J., Sciortino, S., Willingale, R., Wilms, J.: Athena+: The first Deep Universe X-ray Observatory (2013). https://arxiv.org/abs/1310.3814
44. Barret, D., Decourchelle, A., Fabian, A., Guainazzi, M., Nandra, K., Smith, R., Herder, J.-W.: The Athena space X-ray observatory and the astrophysics of hot plasma. Astronomische Nachrichten 341(2), 224–235 (2020) https://doi.org/10.1002/asna.202023782 - https://onlinelibrary.wiley.com/doi/pdf/10.1002/asna.202023782
45. Hitomi Collaboration, Aharonian, F., Akamatsu, H., Akimoto, F., Allen, S. W., Angelini, L., … Zhuravleva, I.: The quiescent intracluster medium in the core of the Perseus cluster. Nature 535(7610), 117–121 (2016). https://doi.org/10.1038/nature18627

Author

Hanna Cho is a junior at Yongsan International School of Seoul, South Korea. She has a passion for hands-on problem solving and loves the challenges of building, designing, or experimenting. With a keen interest in problem-solving and innovation, she is excited to pursue a future in engineering.

DOI: 10.36838/v7i9.37